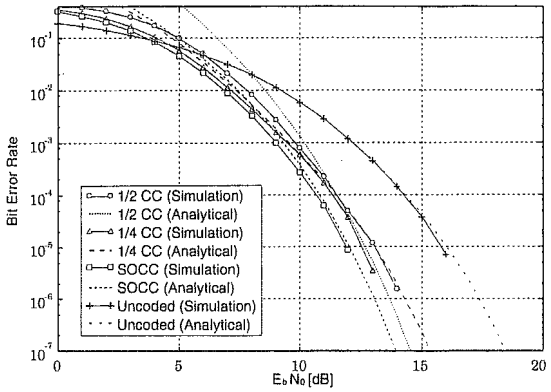

Figure 4: Comparison of BER for different convolutional coding schemes in terms of E_b/N_0 for MRC-RAKE receiver for $L = 8$, N_u=1, $K = 5$, Channel model=CM3.

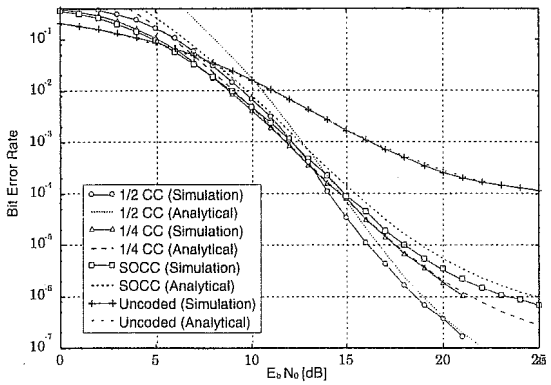

Figure 5: Comparison of BER for different convolutional coding schemes in terms of E_b/N_0 for MRC-RAKE receiver for $L = 8$, N_u=30, $K = 5$, $J = 1$, Channel model=CM3.

and $1/16$ for $K = 6$ from the relationship between constraint length and code rate as mentioned in Section 2.1. In order to make a fair comparison, all codes have the same number of states in trellis diagram. It is equivalent to that each encoders have the same memory length. At the decoder, soft-decision Viterbi decoding is assumed for each schemes. For spreading sequence, we employ Gold sequence. In order to align the total processing gain, we set spreading sequence length as $N_c = 127$ and 63 for rate $1/2$ CC and rate $1/4$ CC, and $N_c = 31$ and 15 for SOCC of rate $1/8$ and $1/16$, respectively. The number of RAKE finger is fixed to $L = 8$ for all schemes. Because of the space limitation, only the result for channel model (CM) 3 is shown.

4.2. Performance for Single-User ISI Channel

Fig. 4 shows the bit error rate (BER) versus SNR per information bit, E_b/N_0, where E_b is the average received energy per information bit and N_0 is spectral density of the AWGN. The solid lines represent Monte-Carlo simulation results for MRC-RAKE receivers, and the dotted lines are analytical upper bound of bit error probability. In our simulations, 30000 bits are sent for each channel and the BER is averaged over 100 multipath channels. In the figure, simulation results are in good agreement with analytical results for all schemes. It is observed that SOCC outperforms $1/2$ CC and $1/4$ CC for all figures because of strong error correction capability, i.e., large free distance.

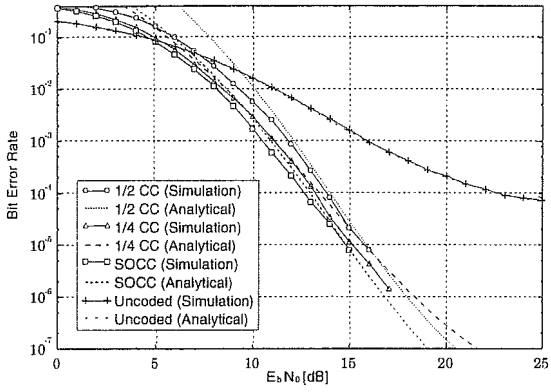

Figure 6: Comparison of BER for different convolutional coding schemes in terms of E_b/N_0 for MRC-RAKE receiver for $L = 8$, N_u=30, $K = 5$, $J = 4$, Channel model=CM3.

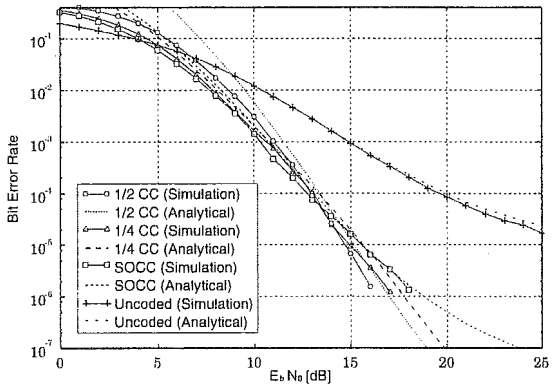

Figure 7: Comparison of BER for different convolutional coding schemes in terms of E_b/N_0 for MMSE-RAKE receiver for $L = 8$, N_u=30, $K = 5$, $J = 1$, Channel model=CM3.

4.3. Performance for Multi-User Channel

Fig. 5-8 show the BER versus E_b/N_0 for multipath and multiple access environment. The number of users is 30. We assume that the received energies of all users are the same, i.e., $A_k = 1$ for all k. Fig. 5 shows the performance for MRC-RAKE receiver using short spreading sequence, i.e., $J = 1$. As shown in the figure, as code rate decreases, the performance gradually degrades except uncoded case. This is because the performance of the system that employ short spreading sequence depends largely on the length of the spreading sequence N_c, as the interference coefficient remain unchanged during the transmission time. Fig. 6 shows the BER performance for MRC-RAKE receiver using code-hopping scheme for $J = 4$. This figure shows that the degradation of the performance due to multiple interference users is reduced, and as code rate decreases, the performance is improved. This is due to the fact that by using multiple spreading sequence, the interference coefficient change from one symbol to another, yielding interference from multiple users close to Gaussian distribution.

Fig. 7 and 8 show the BER performance for MMSE-RAKE combining receiver. Fig. 7 is BER performance for short spreading case, and Fig. 8 shows the BER performance for code-hopping scheme. From these figure, again we can see that by using multiple spreading sequence per single user, the performance for low-rate coded scheme is improved. In addition, by using MMSE-RAKE receiver, the preformance is more improved

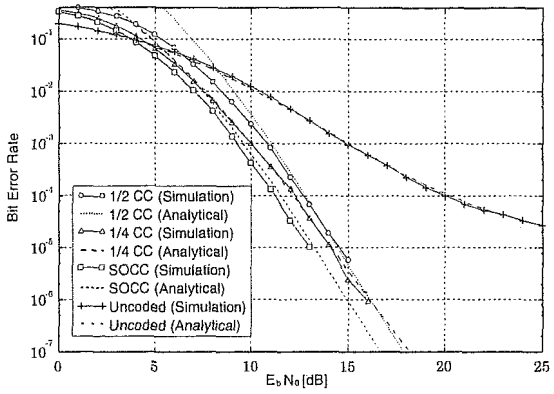

Figure 8: Comparison of BER for different convolutional coding schemes in terms of E_b/N_0 for MMSE-RAKE receiver for $L = 8$, N_u=30, $K = 5$, $J = 4$, Channel model=CM3.

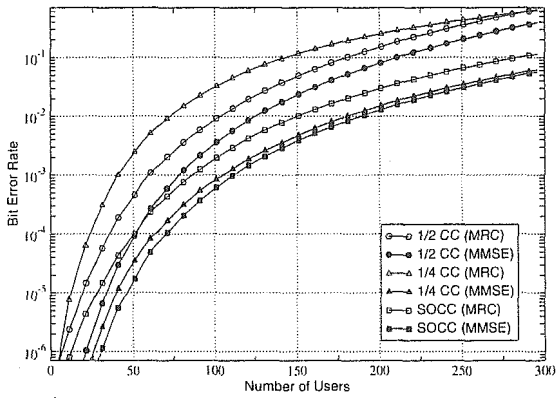

Figure 9: Comparison of BER for different convolutional coding schemes in terms of number of active users for both MRC-RAKE receiver and MMSE-RAKE receiver for $E_b/N_0 = 15$ [dB], $K = 5$, $L = 8$, Channel model=CM3.

comapred to that using MRC-RAKE receiver (Fig. 5 and Fig. 6). This figure tells that MMSE RAKE receiver effectively combine multipath energy and suppress both multi-user interference and inter-symbol interference. Although we employ $L = 8$ here, increasing L leads to more performance improvement. That is a trade-off between performance improvement and implementation complexity.

Fig. 9 shows the average BER versus number of users N_u for fixed $E_b/N_0 = 15$ dB. All lines represent the upper bound. From this figure, we can find that SOCC outperforms $1/2$ CC and $1/4$ CC in multiuser environment for both types of receivers. It should be noted that we consider under fixed total spreading factor, the relative behavior remains unchanged if the load of the system N_u/F changes.

4.4. Spectral Efficiency

Finally, Fig. 10 shows the comparison of achievable spectral efficiency in terms of total spreading factor. Here the spectral efficiency is defined as $N_u R_b$, where N_u denotes maximum number of users to achieve BER= 10^{-4}. We can fined that the lower the code rate, larger system capacity is achievable. In addition, MMSE receiver effectively suppress the interference from other users and incease the system capacity.

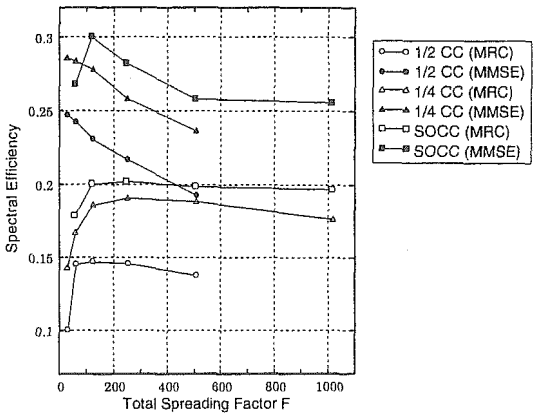

Figure 10: Achievable spectral efficiency in terms of total spreading factor for $E_b/N_0 = 15$[dB], BER=10^{-4}, $L = 8$, $J = 4$, $K = 5$, Channel model=CM3.

5. Conclusions

In this paper, we have studied the use of SOCC to improve the average BER performance of DS-UWB systems over multipath and multiple access environment. We showed that the performance of low-rate codes degrade under multiuser environment due to its poor correlation property of the spreading sequence. In order to combat MUI and ISI, code-hopping scheme is employed in conjunction with low-rate coding to make the interference independent from one symbol to another. The results show that SO coded scheme outperforms the conventional convolutional coded schemes for both types of RAKE receivers, that is, MRC and MMSE combining receivers, for multipath and multiple access channels. In addition, the results suggest that the use of MMSE-RAKE receiver effectively increase the accommodate number of users in a system. We concluded that for low data rate and low cost applications such as low-rate WPANs, combined low-rate coding and code-hopping is suitable. With optional MMSE-RAKE receiver, system capacity further increases.

REFERENCE

[1] M. L. Welborn, "System Considerations for Ultra-Wideband Wireless Networks", Proc. IEEE Radio and Wireless Conf., Boston, MA, Aug. 19-22, 2001.

[2] A. R. Fourouzan, M. Nasiri-Kenari and J. A. Salehi, "Performance Analysis of Time-Hopping Spread-Spectrum Multiple-Access Systems : Uncoded and Coded Schemes", IEEE Tras. on Commun., vol.1, No.4, Oct. 2002.

[3] A. J. Viterbi, CDMA : Principles of Spread Spectrum Communication, AddisonWesley, 1995.

[4] J. G. Proakis, Digital Communications, Mcgraw-Hill 1995.

[5] R. A. Scholtz, "Multiple access with time hopping impulse modulation", in Proc. Military Commun. Conf., pp.447-450, Oct. 1993.

[6] J. Foerster, "Channel Modeling Sub-committee Report Final", IEEE P802.15 Working Group for Wireless Personal Area Networks (WPANs).

[7] J. D.Choi, "Performance of Ultra-Wideband Communications With Suboptimal Receivers in Multipath Channels", IEEE J. Select. Areas Commun., vol.20, no.9, Dec. 2002.

An Adaptive Frame-based Interpolation Method of Channel Estimation for Space-Time Block Codes in Moderate Fading Channels

Gabriel Porto Villardi[†], *Giuseppe Thadeu Freitas de Abreu*[‡] *and Ryuji Kohno*[†]

[†]Department of Electrical and Computer Engineering, Yokohama National University, Yokohama-shi, Hodogaya-ku, Tokiwadai 79-5, 240-8501, Japan.

gabriel.villardi@kohnolab.dnj.ynu.ac.jp and kohno@ynu.ac.jp

[‡]Centre for Wireless Communications, University of Oulu, P. O. Box 4500, 90014-Finland

giuseppe@ee.oulu.fi

Abstract — **The application of Orthogonal Space-Time Block Codes (O-STBC) as the encoding scheme in the presence of "*non-quasi-static*" fading was considered. A simple and efficient adaptive method of channel estimation based on the interpolation of estimates acquired at the pre-amble and post-amble of framed blocks of information is developed. Moreover, the proposed method is proven, both theoretically and by simulations, to outperform the alternative of channel tracking, despite its significant low complexity.**

Keywords — **STBC, Channel Estimation, Interpolation, non-quasi-static fading**

1. Introduction

Since Space-Time Block Codes from Orthogonal Designs were introduced [2], as an extension of Alamouti Codes [3], they have gained a lot of attention due to their potential application in conjunction with multiple-input multiple-output (MIMO) systems.

Despite drawbacks in capacity, as shown in [4], O-STBC is very appealing in terms of complexity and performance. In addition to this, to the best of our knowledge, it is the only STBC technique that can be easily made robust to the *continuous* (rather than block) fluctuation characteristic of *non-quasi-static* fading channels [1], one of the causes of loss of orthogonality in symbol decoding.

Nevertheless, the performance of this improved scheme still relies on accurate channel state information (CSI), which may require the insertion of a large amount of pilot symbols, therefore degrading the overall throughput of the system.

In this paper a simple and accurate method for channel estimation of Space-Time Block Coded OFDM systems, based on adaptive length frame-based interpolation method is proposed. The paper is structured as follows. In section 2, the interpolation technique is justified by an analysis of the influence that the autocorrelation properties of the channel estimates have on the performance of the robust O-STBC scheme [1]. In section 3, the adaptive frame-based interpolation scheme for channel estimation itself is explained. In section 4, theoretical expressions of the SER and BER for coherent schemes of the proposed system using MPSK modulation are also derived. In section 5, the performance of systems employing the proposed technique are compared to those of systems with perfect channel estimation and online channel tracking based on Kalman filter. Finally, conclusions are drawn in section 6.

2. Interference Coefficient Analysis

In this section we analyze the influence of the autocorrelation of the channel estimation on minimizing the interference coefficient resultant from channel estimation errors within a symbol block. In addition to it, we demonstrate that the Linear Maximum Likelihood Decoder [1] benefits from a high-correlated channel estimation, therefore favoring the use of interpolation methods.

As described by [1], fully orthogonal linear symbol decoding in the presence of "*non-quasi-static*" fading channels (hereafter referred as moderate fading) is achieved by successively applying a partial orthogonal decoder, also derived in [1]. If STBC codewords are sent from four transmit antennas in a moderate fading, the estimated symbol, say $\hat{s}_1$, after one step of the partially orthogonal combiner is given by

$$\begin{aligned}\widehat{s}_{1,\tilde{2}} = {} & s_1 h_{1,1}\tilde{h}^*_{1,6} + (\ \ s_2 h_{2,1} + s_3 h_{3,1} + s_4 h_{4,1} + w_1)\tilde{h}^*_{1,6} + \\ & + s_1 h_{2,2}\tilde{h}^*_{2,5} + (-s_2 h_{1,2} - s_4 h_{3,2} + s_3 h_{4,2} + w_2)\tilde{h}^*_{2,5} + \\ & + s_1 h_{3,3}\tilde{h}^*_{3,8} + (-s_3 h_{1,3} + s_4 h_{2,3} - s_2 h_{4,3} + w_3)\tilde{h}^*_{3,8} + \\ & + s_1 h_{4,4}\tilde{h}^*_{4,7} + (-s_4 h_{1,4} - s_3 h_{2,4} + s_2 h_{3,4} + w_4)\tilde{h}^*_{4,7} + \\ & + s_1 h^*_{1,5}\tilde{h}_{1,2} + (\ \ s_2 h^*_{2,5} + s_3 h^*_{3,5} + s_4 h^*_{4,5} + w^*_5)\tilde{h}_{1,2} + \\ & + s_1 h^*_{2,6}\tilde{h}_{2,1} + (-s_2 h^*_{1,6} - s_4 h^*_{3,6} + s_3 h^*_{4,6} + w^*_6)\tilde{h}_{2,1} + \\ & + s_1 h^*_{3,7}\tilde{h}_{3,4} + (-s_3 h^*_{1,7} + s_4 h^*_{2,7} - s_2 h^*_{4,7} + w^*_7)\tilde{h}_{3,4} + \\ & + s_1 h^*_{4,8}\tilde{h}_{4,3} + (-s_4 h^*_{1,8} - s_3 h^*_{2,8} + s_2 h^*_{3,8} + w^*_8)\tilde{h}_{4,3} \quad (1)\end{aligned}$$

where $\widehat{s}_{p,\tilde{q}}$ represents the estimation of s_p, orthogonal to s_q, $h_{m,n}$ and $\tilde{h}_{m,n}$ are the channel m at the transmission instant n and its estimation, respectively, and w denotes a zero-mean white complex Gaussian distributed noise with variance $\sigma^2_w/2$ per dimension.

Based on (1) it is clear that for perfect CSI at the decoder ($h = \tilde{h}$), the coefficient of s_2 vanishes, therefore leading to a partially orthogonal decoding $\widehat{s}_{1,\tilde{2}}$. By successively applying the partially orthogonal combiner, coefficients of s_3 and s_4 also vanish yielding a fully orthogonal decoding $\widehat{s}_{1,\tilde{2},\tilde{3},\tilde{4}}$. Unfortunately, decoders in the real world can not count with perfect channel knowledge, therefore the interference factor of s_q in the estimation of s_p do exist and depends of the accuracy of the estimation method.

Now, knowing that channel estimation errors are also responsible for loss of orthogonality in symbol decoding, one question could arise: what kind of estimation error would

have less impact on the system performance? The one resultant from low-autocorrelated channel estimation methods, such as online tracking algorithms, or the one resultant from high-autocorrelated methods, such as polynomial interpolations?

To answer this question, we start by:

A. Modeling the estimated channel as

$$\tilde{h}_{m,n} = (\sqrt{1-\varepsilon})h_{m,n} + g_{m,n} \tag{2}$$

where g is the estimation error with mean square error (MSE) ε normalized by the variance (power) of the h (σ_h^2). Details of (2) are found at the appendix A.

B. Modeling each channel and estimation error processes as an auto-regressive model [6], therefore consecutive samples of the same process can be related by

$$h_{m,n+u} = \alpha_{m,u}h_{m,n} + v_{m,n} \tag{3}$$

$$g_{m,n+u} = \beta_{m,u}g_{m,n} + k_{m,n} \tag{4}$$

where v_m and k_m are zero-mean complex Gaussian random variables uncorrelated to each other and to all other variables. Also, α and β are the normalized autocorrelation functions of h and g, respectively, and u is the instant difference between the left hand side and the right hand side of (3) and (4). Details of (3) and (4) are found in appendix B.

C. Writing (1) in a simplified form

$$\widehat{s}_{1,\tilde{2}} = s_1 + \frac{bs_2 + cs_3 + ds_4 + w}{a} \tag{5}$$

where a,b,c and d are factors which vary according to the values of $h_{m,n}$ and w represents the sum of the noises in a symbol block.

Due to the multi-step nature of the decoder in [1] a full mathematical analysis of the interference coefficient present in the estimation of s_1 is prohibitively complex. Thus, we focus on the factors $E[b]$ and $E[a]$ after the first step of the partially orthogonal combiner, leading to a simpler though efficacious analysis. As b is existent due to channel estimation errors, it propagates through all the steps of the decoder, resulting in a final non orthogonal estimation of s_1. Above, $E[\cdot]$ denotes expected value.

C.1. Gain Factor a

$$\begin{aligned} a = {} & (\beta_{1,4}g^*_{1,2} + z_1)h_{1,1} + g_{2,1}(\alpha_{2,4}h^*_{2,2} + r_2) + \\ & + g_{1.2}(\alpha_{1,4}h^*_{1,1} + r_1) + (\beta_{2,4}g^*_{2,1} + z_2)h_{2,2} + \\ & + (\beta_{3,4}g^*_{3,4} + z_3)h_{3,3} + g_{4,3}(\alpha_{4,4}h^*_{4,4} + r_4) + \\ & + (\beta_{4,4}g^*_{4,3} + z_4)h_{4,4} + g_{3,4}(\alpha_{3,4}h^*_{3,3} + r_3) + \\ & + (\sqrt{1-\varepsilon})(h_{1,1}h^*_{1,6} + h_{2,2}h^*_{2,5} + h_{3,3}h^*_{3,8} + \\ & + h_{4,4}h^*_{4,7} + h^*_{1,5}h_{1,2} + h^*_{2,6}h_{2,1} + h^*_{3,7}h_{3,4} + \\ & + h^*_{4,8}h_{4,3}) \end{aligned} \tag{6}$$

C.2. Interference Factor b

$$\begin{aligned} b = {} & (\beta_{1,4}g^*_{1,2} + z_5)h_{2,1} - g_{2,1}(\alpha_{1,4}h^*_{1,2} + r_5) + \\ & + g_{1,2}(\alpha_{2,4}h^*_{2,1} + r_6) - (\beta_{2,4}g^*_{2,1} + z_6)h_{1,2} + \\ & - (\beta_{3,4}g^*_{3,4} + z_7)h_{4,3} + g_{4,3}(\alpha_{3,4}h^*_{3,4} + r_8) + \\ & + (\beta_{4,4}g^*_{4,3} + z_8)h_{3,4} - g_{3,4}(\alpha_{4,4}h^*_{4,3} + r_7) \end{aligned} \tag{7}$$

Where z_x and $r_x, \forall x \in \{1,2,3,4,5,6,7,8\}$, are mutually uncorrelated, zero-mean Gaussian random variables. Derivation of (6) and (7) are found at the appendix C.

By analyzing equation (6) and (7), it is obvious that interference factor $E[b]$ and gain factor $E[a]$, which are related to the final interference coefficient, are dependent on β, the autocorrelation of the estimation error, therefore being dependent on the channel estimation method applied .

From figure (1) and (2) it can be noticed that, for higher values of $\beta_{m,u}$, the interference factor b slightly decreases while the gain factor a has a slight increment, for the same values of channel estimation's mean square error Υ. The behavior of these two factors, qualitatively, tells us the advantage of using high-autocorrelated channel estimation methods (leading to higher $\beta_{m,u}$ values), although it does not give us a clear figure of how important these slight improvements will be to reduce the final interference coefficient. Thus, the previous mathematical analysis requires a completion which could be achieved through computational evaluation. The computation of the final interference is shown in figure (3).

As expected, figure (3) indicates that for the same values of Υ, the higher β is, the smaller is the final interference coefficient influencing the final system performance. Therefore, the use of polynomial interpolation methods is favored. In appendix D the reader can enjoy a mathematical analysis of the relationship between the autocorrelations of the channel estimation and channel estimation error processes.

3. Proposed Estimation Method

In this section we propose a channel estimation method consisting of an adaptive length frame-based higher order Lagrangean estimator providing CSI to the Orthogonal Linear Maximum Likelihood Decoder [1] applied to OFDM technology. Here, we describe the system based on a more realistic time-selective, though frequency flat channel of a single OFDM subcarrier.

Since mobile units (MU) are on the move, the severity of the fading they are exposed to is constantly changing. Thus, a channel estimation method which adjusts its frame length according to the Doppler frequency seen by the MUs, avoiding interpolation divergence, will obviously be more desirable than fixed length methods.

The estimation method is subdivided in two parts: The training mode to acquire $h_{m,n}$ values at the pilots and the adaptive length frame-based interpolation mode. In the scope of this paper we are focusing only on the second one, letting the first mode be provided by any known method such as the ones developed in [8].

1. Lagrange Interpolation

For a given set of data points (t_i, h_i) where t_i represents the pilot time-slots (TS) and h_i, the real/imaginary channel values at the same TS, the Lagrange interpolating polynomial for channel estimation is given by:

$$P(t) = \sum_{i=1}^{n+1} P_i(t) \tag{8}$$

where

$$P_i(t) = h_i \prod_{\substack{k=1 \\ k\neq i}}^{n+1} \frac{t - t_k}{t_i - t_k} \tag{9}$$

$P(t)$ is our n^{th} order polynomial which passes through the points $h_1, h_2, ..., h_{n+1}$. Due to the nature of our application, the pilots are bunched to both extremities of our frame not letting Lagrange Interpolation suffer from Runge's Phenomenon, as seen in [7]. This prevents our channel estimation from diverging wildly from the actual channel as it approaches the data points, even when dealing with higher-order interpolations.

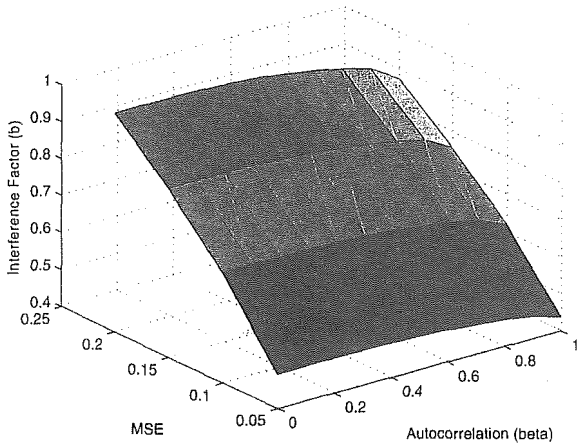

Figure 1: Normalized Interference factor b, after first step of partially orthogonal combiner, for different values of β and mean square error values, for a four transmit antennas system.

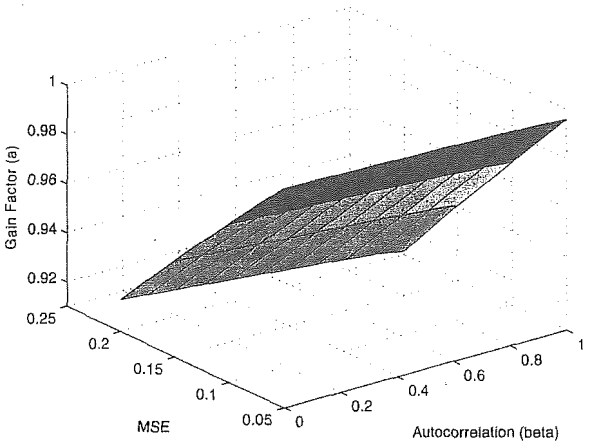

Figure 2: Normalized Gain Factor a, after first step of partially orthogonal combiner, for different values of β and mean square error values, for a four transmit antennas system.

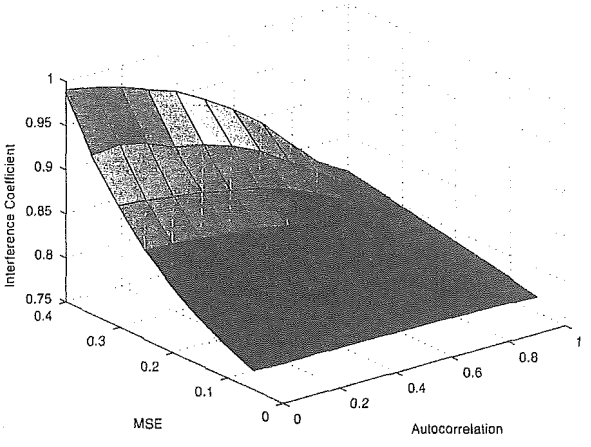

Figure 3: Interference coefficient for different values of β and mean square error values, for a four transmit antennas system in noise.

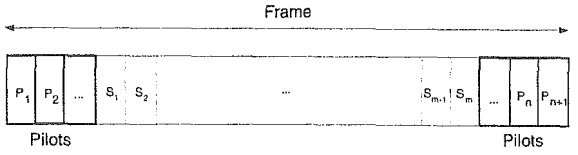

Figure 4: $n+1$ pilots (n = interpolation order) and m O-STBC encoded symbols in a frame.

2. Frame Size Determination

In a mobile environment, in order to achieve a precise channel estimation based on interpolation, it is necessary to have a certain criterion on how to determine the frame size in which the interpolation will occur. For low fading rates, time-selectivity is not so severe, thus longer frames should be employed. On the other hand, in high fading rate scenarios shorter frames yield higher estimation accuracy, though reducing the system throughput.

Our criterion for assuring no interpolation divergence is to employ frames allowing either one *peak* or one *trough* (fade) of the actual real/imaginary channel within its length. However, the challenge is how to determine this length in a simple and effective way, which could be implemented in low cost and small sized terminals. Since the *in-phase* and *quadrature* channels are interpolated separately, we can solve this problem by using the level-crossing ratio theory of Gaussian stochastic processes. As described by [10], the expected number of zeros crossings of a stationary Gaussian process with twice differentiable autocorrelation function, $r(\tau) = E[h_{m,n}h^*_{m,n+\tau}]\sigma^2_{h_m}$, is given by

$$E[N] = \frac{T}{\pi}\sqrt{\left(\frac{-r''(0)}{r(0)}\right)\left(\exp\frac{-\mu^2}{2r(0)}\right)} \tag{10}$$

where τ represents the instant difference of the same channel, N is the number of zero (level) crossings, T represents the considered time length and μ is the mean process value. Since *peak/trough* of the original stochastic Gaussian process (imaginary/real part of the channel) are equivalent to zeros of the derivative of the original process, our task reduces to determining the expected number of zero crossings of the differentiated process $E[N_d]$, since the theoretical frame length FL can easily be calculated by

$$FL = \frac{1}{E[N_d]}. \tag{11}$$

Also, differentiation is a linear process, therefore the derivative of a stochastic Gaussian process remains a stochastic Gaussian process. Although, the autocorrelation of the differentiated process becomes

$$r_d(\tau) = J_0(2\pi Fm\tau\Delta t)\sigma_d^2 \tag{12}$$

where J_0 is the Bessel function of the first kind, σ_d^2 refers to the variance of the process after the differentiation, Fm is the maximum Doppler frequency and Δt is a constant representing the time lag between consecutive symbol transmissions, in other words, the transmit symbol duration.

Let T be the unity of time and reminding that μ is zero for both the process and its derivative, (10) can be reduced to

$$E[N] = \frac{1}{\pi}\sqrt{\left(\frac{-r_d''(0)}{r_d(0)}\right)} \tag{13}$$

where $r''_d(0)$ can be calculated as follows:

let

$$C = 2\pi Fm\Delta t \tag{14}$$

then

$$\begin{aligned} 2J'_0(C\tau) &= \big(J_{-1}(C\tau) - J_1(C\tau)\big)C \\ J''_0(C\tau) &= \frac{1}{2}\big(J'_{-1}(C\tau) - J'_1(C\tau)\big)C \\ &= \frac{1}{2}\Big[\frac{1}{2}\big(J_{-2}(C\tau) - J_0(C\tau)\big) - \frac{1}{2}\big(J_0(C\tau) - J_2(C\tau)\big)\Big]C^2 \\ &= \frac{1}{2^2}[J_{-2}(C\tau) - 2J_0(C\tau) + J_2(C\tau)]C^2. \end{aligned} \tag{15}$$

Since $J_{-2}(C\tau) = J_2(C\tau)$; $J_2(C\tau) = 0$ and $J_0(C\tau) = 1$ for $\tau = 0$,

$$J''_0(0) = \frac{1}{2^2}[-2C^2] \tag{16}$$

and

$$r_d(0) = \sigma_d^2 \tag{17}$$

$$r''_d(0) = -2(\pi Fm\Delta t)^2\sigma_d^2. \tag{18}$$

Thus

$$E[N_d] = Fm\Delta t\sqrt{2} = \frac{Fm\sqrt{2}}{Sr} \tag{19}$$

$$FL = \frac{Sr}{\sqrt{2}\,Fm} \tag{20}$$

where FL is, in average, the frame size (information symbols), Sr, the symbol rate (symb/s) of each subcarrier of the OFDM system and Fm represents the maximum doppler frequency (Hz) resultant from the mobile unit's movement.

4. Theoretical Symbol and Bit Error Rates

In this section the exact symbol error rate and well approximated bit error rates expressions for the coherent scheme of the proposed system are derived.

$$P_{symb} = \frac{1}{\pi}\int_0^{\frac{(M-1)\pi}{M}} \prod_{l=1}^{4} M_{\gamma_l}\Big(\frac{-g}{sin^2\phi}\Big)d\phi \tag{21}$$

$$P_{bit} \approx \frac{P_M}{k} \tag{22}$$

Where M represents the constellation size; M_{γ_l} is the Moment Generating Function MGF of the SNR per symbol γ_l associated with the path l; g is $J_0(2\pi 3\Delta t Fm)$ when l assumes either the values 1 or 2 and $J_0(2\pi 5\Delta t Fm)$ when l is either 3 or 4. Also J_0 represents the Bessel function of the first kind.

5. Performance Analysis and Simulations

In this section we show some relevant results confirming the efficacy of the proposed technique. We propose a 30 Mbits/s Space-Time Block Coded OFDM system with central frequency of 5 GHz, 1024 subcarriers, each transmitting at a data rate of 29295 bits/sec and 8-QPSK modulation.

All simulations in this paper followed the Jakes Model to generate channels with maximum Doppler frequency (Fm) of 50 Hz. In addition to this, O-STBC with four transmit antennas was used as the coding scheme and 7^{th} order Lagrange interpolation was adopted.

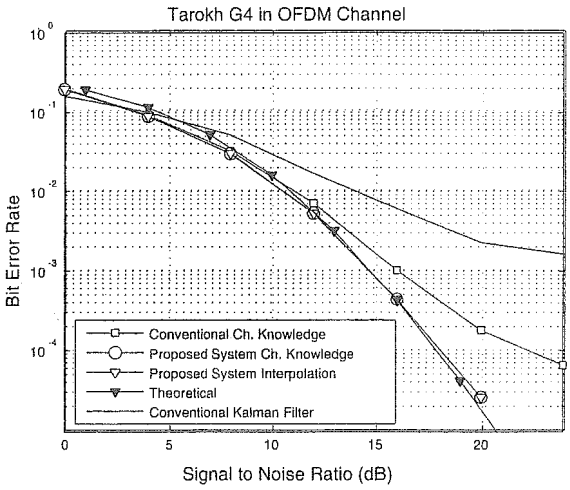

Figure 5: BER comparison between different systems and theory

In figure (5) we can see that the proposed system achieves an improved performance when compared to the conventional decoder using Kalman filter as the channel estimator and even when the latter benefits from perfect channel knowledge. In addition to this, it can be seen that the use of 7^{th} order Lagrange interpolation as the channel estimator does not significantly affect the performance of the proposed system when compared to the case of perfect channel knowledge. Also, by examining figure (6), the difference between the quality of channel estimation provided by proposed method and the online channel tracking (Kalman filter), becomes obvious. Moreover, we can see the provided theoretical and simulated BER curves of the proposed system are in conformity.

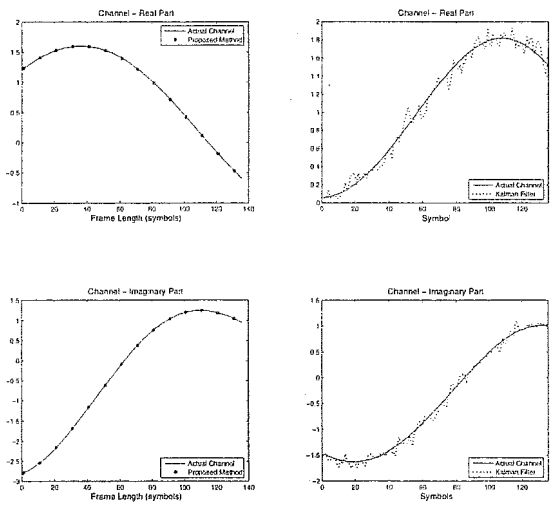

Figure 6: Channel estimation by the proposed method and Kalman Filter with 100 iterations (15 dB).

6. Conclusions

An efficient and low complexity adaptive length frame based interpolation method which significantly improves the quality of channel estimation in the constantly changing scenario of mobile communication systems is proposed, allowing MUs to seamlessly range from low to high fading rates

situations. As a consequence, the problem emergent from the application of O-STBC as the encoding scheme in the presence of "*moderate*" fading channels is combated. Moreover, the proposed system clearly outperforms the conventional one, even when the latter benefits form perfect CSI. In addition to this, exact theoretical expressions for SER and well approximated for BER computation of the proposed system are provided.

A. Appendix

$$g_{m,n} = h_{m,n} - \tilde{h}_{m,n} \tag{23}$$

$$\Upsilon = E[|h_{m,n} - \tilde{h}_{m,n}|^2] = E[|g_{m,n}|^2] \therefore \Upsilon = \sigma^2_{g_{m,n}} \tag{24}$$

Where $E[\cdot]$ denotes expected value. Let

$$\Upsilon = \varepsilon \sigma^2_{h_{m,n}} \tag{25}$$

Then, ε is the normalized mean square error. We can verify the consistency of (2), by checking its variance (power) equivalence

$$\begin{aligned} \sigma^2_{h_{m,n}} &= (1-\varepsilon)\sigma^2_{h_{m,n}} + \sigma^2_{g_{m,n}} \\ \sigma^2_{\tilde{h}_{m,n}} &= \sigma^2_{h_{m,n}} \end{aligned} \tag{26}$$

What was already expected, since channel estimates can not suffer an increment of power, whatsoever.

B. Appendix

As described by [6], if the fading rate is not so fast, then, (3) and (4) hold. The variance of $v_{m,n}$ ($\sigma^2_{v_{m,n}}$) and $k_{m,n}$ ($\sigma^2_{k_{m,n}}$) are given by $(1-\alpha^2_{m,u})\sigma^2_{h_{m,n}}$ and $(1-\beta^2_{m,u})\Upsilon$, respectively. Consistency of (3) can be checked by its variance equivalence

$$\begin{aligned} \sigma^2_{h_{m,n+u}} &= \alpha^2_{m,u}\sigma^2_{h_{m,n}} + (1-\alpha^2_{m,u})\sigma^2_{h_{m,n}} \\ \sigma^2_{h_{m,n+u}} &= \sigma^2_{h_{m,n}} \end{aligned} \tag{27}$$

As expected the channel variance does not depend on the time instant n, thus its notation can be simplified to $\sigma^2_{h_m}$. Consistency of (4) can be checked by the same procedure

$$\begin{aligned} \sigma^2_{g_{m,n+u}} &= \beta^2_{m,u}\Upsilon + (1-\beta^2_{m,u})\Upsilon \\ \sigma^2_{g_{m,n+u}} &= \sigma^2_{g_{m,n}} = \sigma^2_{g_m} = \Upsilon \end{aligned} \tag{28}$$

By (28) it is clear that (4) models the channel estimation error process with a normalized autocorrelation function β and mean square error Υ.

C. Appendix

By simply rearranging (1), gain factor a and interference factor b can be, respectively, written as

$$\begin{aligned} a &= h_{1,1}\tilde{h}^*_{1,6} + h_{2,2}\tilde{h}^*_{2,5} + h_{3,3}\tilde{h}^*_{3,8} + h_{4,4}\tilde{h}^*_{4,7} + \\ &+ h^*_{1,5}\tilde{h}_{1,2} + h^*_{2,6}\tilde{h}_{2,1} + h^*_{3,7}\tilde{h}_{3,4} + h^*_{4,8}\tilde{h}_{4,3} \end{aligned} \tag{29}$$

$$\begin{aligned} b &= h_{2,1}\tilde{h}^*_{1,6} - h_{1,2}\tilde{h}^*_{2,5} - h_{4,3}\tilde{h}^*_{3,8} + h_{3,4}\tilde{h}^*_{4,7} + \\ &+ h^*_{2,5}\tilde{h}_{1,2} - h^*_{1,6}\tilde{h}_{2,1} - h^*_{4,7}\tilde{h}_{3,4} + h^*_{3,8}\tilde{h}_{4,3} \end{aligned} \tag{30}$$

Making use of the models described in (3) and (4)

$$\begin{aligned} h_{1,1}\tilde{h}^*_{1,6} &= h_{1,1}(\sqrt{1-\varepsilon}h^*_{1,6} + g^*_{1,6}) \\ &= h_{1,1}(\beta_{1,4}g^*_{1,2} + z_1) + h_{1,1}h^*_{1,6}\sqrt{1-\varepsilon} \end{aligned} \tag{31}$$

$$\begin{aligned} h^*_{1,5}\tilde{h}_{1,2} &= h^*_{1,5}(\sqrt{1-\varepsilon}h_{1,2} + g_{1,2}) \\ &= g_{1,2}(\alpha_{1,4}h^*_{1,1} + r_1) + h^*_{1,5}h_{1,2}\sqrt{1-\varepsilon} \end{aligned} \tag{32}$$

Where z_x and $r_x, \forall x \in \{1,2,3,4,5,6,7,8\}$, are mutually uncorrelated, zero-mean Gaussian random variables with variance $(\sigma^2_{g_m} - \beta^2_{m,u}\sigma^2_{g_m})$ and $(\sigma^2_{h_m} - \alpha^2_{m,u}\sigma^2_{h_m})$, respectively. By modeling all elements of (29) and (30) as done in (31) and (32), (6) and (7) are derived.

D. Appendix

$$\begin{aligned} \gamma_{m,u} &= \frac{1}{\sigma^2_{\tilde{h}}} E[\tilde{h}_{m,n}\tilde{h}^*_{m,n+u}] \\ &= \frac{(1-\varepsilon)}{\sigma^2_{\tilde{h}}} E[(h_{m,n} + g_{m,n})(h^*_{m,n+u} + g^*_{m,n+u})] \\ &= \frac{(1-\varepsilon)}{\sigma^2_{\tilde{h}}} (E[h_{m,n}h^*_{m,n+u}] + E[g_{m,n}g^*_{m,n+u}]) \\ &= \frac{(1-\varepsilon)}{\sigma^2_{\tilde{h}}} (\alpha_{m,u}\sigma^2_{h_m} + \beta_{m,u}\sigma^2_{g_m}) \\ &= (1-\varepsilon)(\alpha_{m,u} + \beta_{m,u}\varepsilon) \end{aligned} \tag{33}$$

Above, $\gamma_{m,u}$ is the normalized autocorrelation function of the estimated channel, given by $J_0(2\pi F m u \Delta t)$, where J_0 represents the Bessel function of the first kind, Fm is the maximum Doppler frequency, Δt is the transmit symbol duration and u, the time instant difference. From (33) we can clearly notice the relationship between the autocorrelation function of the channel estimation process $\gamma_{m,u}$ and of the channel estimation error process, $\beta_{m,u}$. Therefore we can conclude that for fixed values of $\alpha_{m,u}$, higher values of $\gamma_{m,u}$ (as the ones generated by polynomial interpolation methods) yield higher values of $\beta_{m,u}$, generating smaller interference coefficient as indicated by figure (3). This will consequently lead to less degradation of the final system performance.

References

[1] G. T. F. de Abreu, H. Ochiai and R. Kohno, "Linear Maximum Likelihood Decoding of Space-Time Block Coded OFDM systems for Mobile Communications," *IEE Proceedings on Communications - Special Issue on Wireless LAN Systems and Internetworking*, Vol. 151, December 2004.

[2] V. Tarokh, H. Jafarkhani and A. R. Calderbank, "Space-Time block Codes from Orthogonal Designs," *IEEE Transactions on Information Theory*, Vol. 45, No. 5, pp. 1456-1467, July 1999.

[3] S. M. Alamouti, "A Simple Transmit Diversity Technique for Wireless Communications," *IEEE Journal on Selected Areas in Communications*, Vol. 16, No. 8, pp. 1451-1458, October 1998.

[4] S. Sandhu and A. Paulraj,"Space-time block codes: a capacity perspective," *IEEE J COML*, Vol. 4, No. 12, pp. 384 - 386, December, 2000.

[5] X. Li, T. Luo, G. Yue, and C. Yin, "A Squaring Method to Simplify the Decoding of Orthogonal Space-Time Block Codes," *IEEE Transactions on Communications*, Vol. 49, No. 10, pp. 1700 - 1703, October 2001.

[6] Z. Liu, X. Ma and G. B. Giannakis, "Space-time coding and Kalman filtering for diversity transmissions through time-selective fading channels," *MILCOM 2000 - IEEE Military Communications Conference*, no. 1, pp. 382 - 386, October 2000.

[7] M. T. Heath, *Scientific Computing: An Introductory Survey*. McGraw-Hill, 2002.

[8] M. K. Tsatsanis, G. B. Giannakis, and G. Zhou, "Estimation and equalization of fading channels with random coefficients," *Signal Processing*, vol. 53, no. 2/3, pp. 211 228, 1996.

[9] W. C. Jakes, *Microwave Mobile Communication*. New York, NY: Wiley, 1974.

[10] K. Ito, "The expected number of zeros of continuous stationary Gaussian processes", *J. Math. Kyoto Univ.* 3 (1963/1964) 207216; MR0166824 (29 #4097).

Non-linear swept chirp waveforms for UWB multiple access communication and ranging

Shumpei Ida, Ryuji Kohno

Division of Electrical and Computer Engineering, Yokohama National University
79–5 Tokiwadai, Hodogaya, Yokohama, 240–8501, Japan.

E–mail: ida@kohnolab.dnj.ynu.ac.jp, kohno@ynu.ac.jp

Abstract— **In this paper we propose a novel multiple access technique utilizing non-linear swept chirp waveforms. The proposed scheme enables multiple access by assigning each user a distinct frequency sweep function. This paper compares performance of DS-UWB and the proposed chirp modulation technique as a communication and ranging system. Simulation results show that the proposed system achieves better performance of communication and ranging in multi-user environment.**

Key words: non-linear sweep, chirp waveform, multiple access, communication and ranging

1. Introduction

Ultra wideband (UWB) has been the focus of much research and development. Since an unique nature of UWB lies in its dual capabilities - communication and ranging, the application to a sensor network is expected in recent years.

Although the one of popular UWB system is using impulses, we paid attention to the chirp waveform originally used for the radar systems. A chirp waveform can occupy such an ultra wide bandwidth as well as impulses [1]. And it has a good peak to average ratio (PAPR) characteristics, and fits a spectrum mask easily. However, since chirp waveform is a long time signal, it is difficult to make multiple access connection which utilizing PN sequences etc. like impulse based system. In [2], Cook has proposed the use of different modulation slope chirps for multi-user applications. The different modulation slope chirps have different bandwidths. It causes degradation of performance. In [3], El-Khamy has proposed the set of chirps which has equal bandwidth. Since the linear frequency swept chirp waveform is used in such systems, when equal frequency sweep pattern collides, the performance deteriorates in asynchronous environment between users.

In this paper, we propose a novel multiple access method utilizing non-linear swept chirp waveforms, and compare performance with DS-UWB system [4]. Because of good correlation characteristics, in multi-user or multi simultaneous operation piconets (SOP) environment [5], simulation results show that the proposed method has better performance of communication and ranging than DS-UWB system.

2. Communication and Ranging System

In order to calculate the distance, it is required to measure the time that is from transmitting a signal to detecting the reflected. When measured time is set to τ, the distance X is $c\tau/2$. The principle of ranging is illustrated in Figure 1.

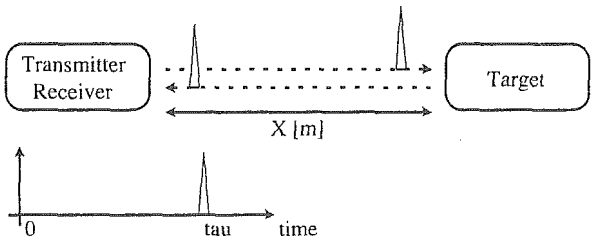

Figure 1: The principle of ranging.

It is necessary to narrow width of a signal for improving axial resolution. However, when peak transmit power is restricted, detection distance will decrease. It solves by using the signal which has good correlation characteristics in the system such as DS-UWB or chirp modulation.

These methods can perform communication and ranging simultaneously in one system by modulating a transmitted signal with data. The communication and ranging system is illustrated in Figure 2.

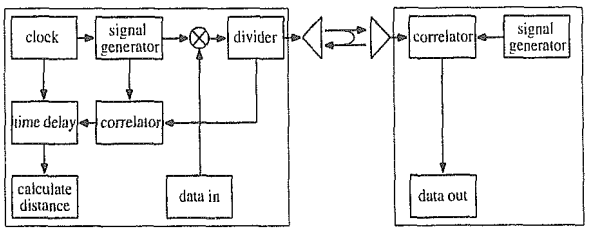

Figure 2: Communication and ranging system.

2.1. DS-UWB

In DS-UWB systems, the pulses are transmitted continuously according to a spreading code [4]. The transmitted signal using BPSK modulation can be expressed as (1).

$$s^{(k)}(t) = \sum_{j=-\infty}^{\infty} \Gamma_j^{(k)} \beta^k_{\lfloor j/N_s \rfloor} w_{tr}(t - jT_f) \qquad (1)$$

The main parameters are:

$w_{tr}(t)$	: Transmitted basic pulse shape.
T_f	: Frame time.
$\Gamma_j^{(k)}$	: Spreading code sequence. ($\Gamma_j^{(k)} \in \{\pm 1\}$)
N_s	: Spreading factor of the system.
$\beta_j^{(k)}$	: Information bit. ($\beta_j^{(k)} \in \{\pm 1\}$)

An example of DS-UWB signal is illustrated in Figure 3.

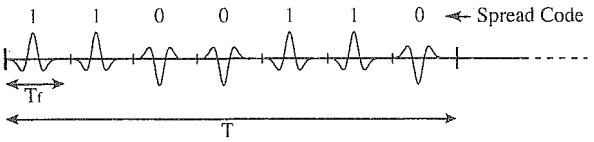

Figure 3: DS-UWB signal.

2.2. Chirp modulation

The general form of chirp signals is given by

$$s^{(k)}(t) = \begin{cases} \cos\left[2\pi \int f_M(t)dt\right] & 0 \le t \le T \\ 0 & otherwise \end{cases} \qquad (2)$$

where $f_M(t)$ and T donate the frequency sweep function and symbol time, respectively [1]. A general linear swept chirp signal and corresponding instantaneous frequency are shown in Figure 4.

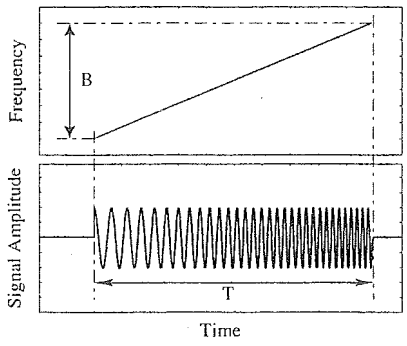

Figure 4: Chirp signal and its instantaneous frequency.

The frequency spectrum characteristics of a linear swept chirp signal is expressed by the so-called Fresnel integrals. Figure 5 shows the spectrum where $BT = 100$. This figure shows that a chirp waveform has an advantage of being easy to match a spectrum mask by rectangular spectrum form.

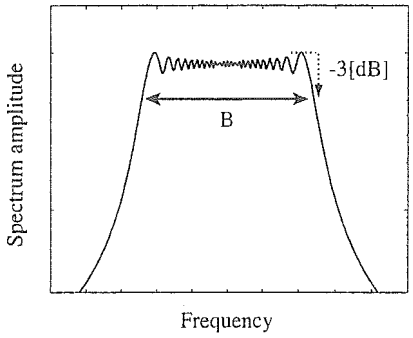

Figure 5: The spectrum of a linear sweep chirp waveform.

If a chirp waveform is fed into its matched filter whose impulse response is also a chirp waveform, but with its frequency varying is the opposite direction, then the output signal typically has a narrow RF peak at the chirp center frequency. This process is called pulse compression. The output waveform of linear swept chirp waveform $g(t)$ is the auto-correlation function of the chirp waveform, and is given by

$$g(t) = \sqrt{BT} \frac{\sin\left\{\pi Bt\left(1 - \frac{|t|}{T}\right)\right\}}{\pi Bt} \cos(2\pi f_0 t) \qquad (3)$$

for $-T < t < T$. This is illustrated in Figure 6.

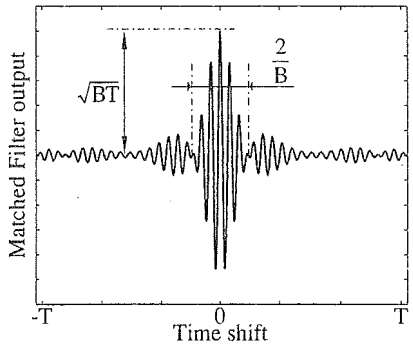

Figure 6 The auto-correlation function of a linear sweep chirp waveform.

3. NON-LINEAR SWEPT CHIRP WAVEFORMS FOR MULTIPLE ACCESS

Generally linear swept chirp waveform is used for radar etc., however it cannot achieve multiple access if all users use an equal waveform. Then the system which assigns each user a unique sweep function have been proposed [3]. Since the frequency which each user uses differs in almost all time, it can achieve multiple access. Although, when it assumes an asynchronous environment between users, multiple access interference has a significant impact on performance. It is because the cross-correlation coefficients between users becomes large when gradient of a sweep function is equal.

Against the problem, multiple access interference, we proposed the system which uses non-linear swept chirp waveforms [6]. By using non-linear sweep functions, since all users will use different frequency in almost all time shifts, low cross-correlation coefficients is achieved. Although the function of several forms was investigated, in this paper, we uses tangent function which auto-correlation characteristic is suitable for ranging [7]. The function assigned to users is defined as

$$\begin{cases} f_M^{(2i-1)}(t) \\ \quad = f_0 + \dfrac{B}{2}\left[1 + \dfrac{1}{\tan(\gamma_i)} \cdot \tan\left\{\dfrac{2\gamma_i}{T}\left(t - \dfrac{T}{2}\right)\right\}\right] \\ f_M^{(2i)}(t) \\ \quad = f_0 + \dfrac{B}{2}\left[1 + \dfrac{1}{\gamma_i} \cdot \arctan\left\{\dfrac{2\tan(\gamma_i)}{T}\left(t - \dfrac{T}{2}\right)\right\}\right] \end{cases} \tag{5}$$

$$i = 1 \cdots M/2 \ (M : \text{number of users}),$$

where γ_i is the parameter which determines the form of the sweep functions. The non-linear sweep functions are selected such symmetrical function (arctangent) which can occupy a spectrum uniformly in the whole system.

The parameter which minimizes a multiple access interference must be chosen. The cause of the interference is the cross-correlation coefficient ρ_{ij}, given by

$$\rho_{ij}(\tau) = \int_0^T s_i(t+\tau)s_j(t)\ dt \tag{6}$$

where τ and T is a time shift between signals and a symbol time respectively. In order to minimize the interference, it is necessary to minimize the maximum value of the cross-correlation coefficient of all combination. The evaluation criteria is given by

$$f(\gamma) = \max_{i \neq j} \max_{0 \leq \tau < T} |\rho_{ij}(\tau)| \quad \longrightarrow \quad \text{Minimization.} \tag{7}$$

This problem is a non-linear optimization problem of many variables. Although it can generally solve with the steepest descent method or the Newton method, since the evaluation function cannot be formulized, it cannot solve using such methods. So, in this paper, the suboptimal combination of parameters is obtained by the direct search method which uses numerical calculation. Results are shown in table I.

Table I: Parameters for non-linear frequency sweep functions.

	γ_1	γ_2	γ_3	γ_4
4 users	1.0479	1.5594	—	—
6 users	0.8054	1.2645	1.5394	—
8 users	0.6287	1.1174	1.3575	1.5437

Proposed non-linear sweep functions assigned to users are shown in Figure 7 (for 6 users).

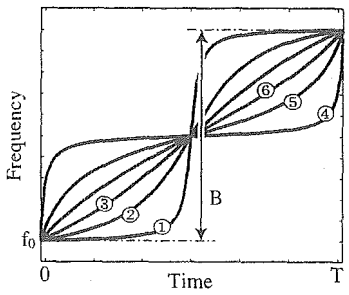

Figure 7: Non-linear sweep functions for multiple access (for 6 users).

4. SIMULATION RESULTS

We show simulation results to compare performance of the proposed scheme and DS-UWB system. The parameter values of the simulations are shown in Table II. An asynchronous environment between users is assumed.

Table II: Simulation parameters.

Data rate	1 [Mbps] (symbol time 1[μs])
Sampling time	0.05 [ns]
Bandwidth	2 [GHz] (3.1~5.1 [GHz])
Modulation scheme	BPSK
Channel	AWGN
Spreading code	M sequence (length 127)
Sweep function	tan · arctan

The signals of each system is illustrated in Figure 8.

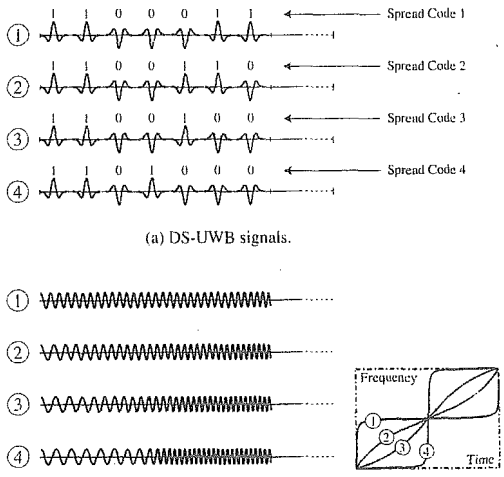

(a) DS-UWB signals.

(b) Proposed non-linear swept chirp signals.

Figure 8: The signals of each system.

4.1. Correlation characteristics

The correlation characteristics of each system are shown in Figure 9 and 10.

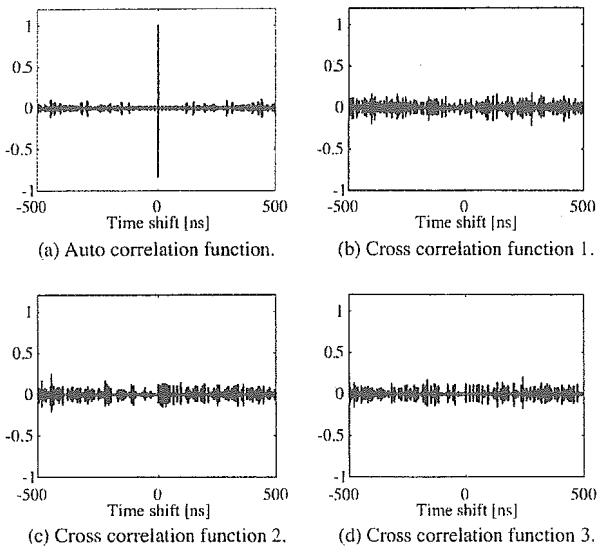

(a) Auto correlation function. (b) Cross correlation function 1.

(c) Cross correlation function 2. (d) Cross correlation function 3.

Figure 9: Correlation characteristics of DS-UWB.

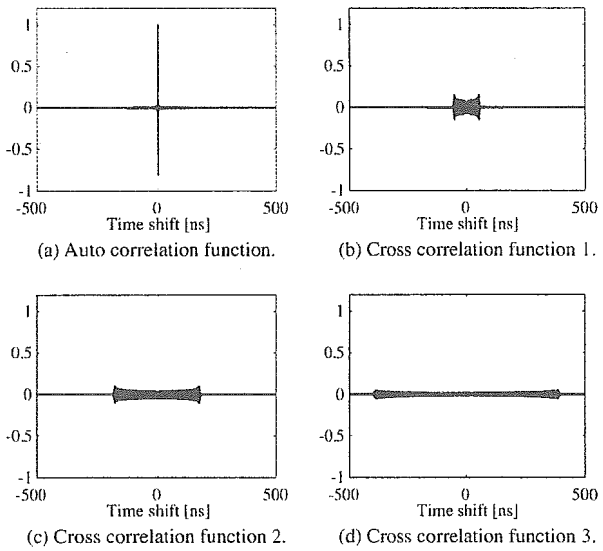

(a) Auto correlation function. (b) Cross correlation function 1.

(c) Cross correlation function 2. (d) Cross correlation function 3.

Figure 10: Correlation characteristics of proposed chirp modulation.

It shows that the proposed system has low sidelobe of the auto-correlation function and low cross-correlation coefficients. The auto-correlation function which has low sidelobe leads a ranging system with few errors and low cross-correlation coefficients leads a robust system against multi-user interference.

4.2. Performance of communication

Bit Error Rate (BER) characteristics in a multiuser environment is shown for a performance evaluation.

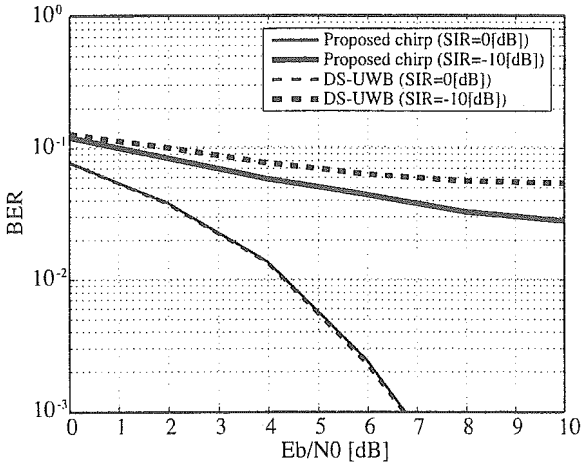

Figure 11: Performance of communication to Eb/N0 (8 users).

Figure 11 shows the BER characteristics to Eb/N0 in multi-user environment (8 users). The desired signal power to interference signal power ratio (SIR) is set as 0 [dB] and -10 [dB]. It shows that the two system is the same communication performance when there is little interference from other users, and the proposed system achieves better performance in furious multiple access interference environment. It is because the proposed signals has low cross-correlation coefficients.

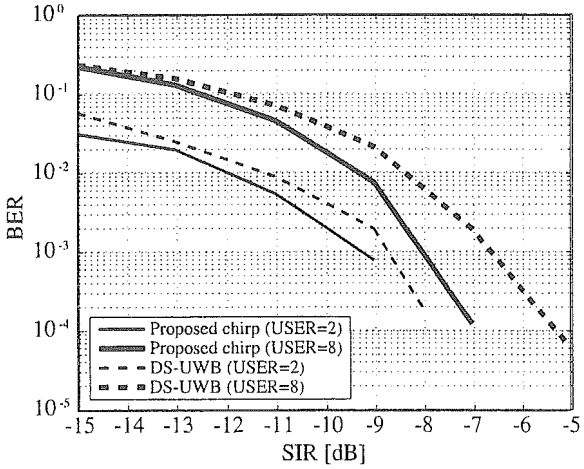

Figure 12: Performance of communication to SIR.

In order to evaluate the effect of a multiple access interference, BER characteristics to SIR is shown in Figure 12. It is assumed that there is no noise source. It shows that

the proposed system is robust in a multi-user environment as compared with DS-UWB system.

4.3. Performance of ranging

In the simulation, a distance is calculated with the use of a time delay which is obtained by detecting a peak point of the correlator output. In addition, the root mean square error (RMSE) is calculated as an evaluation criteria of the ranging performance.

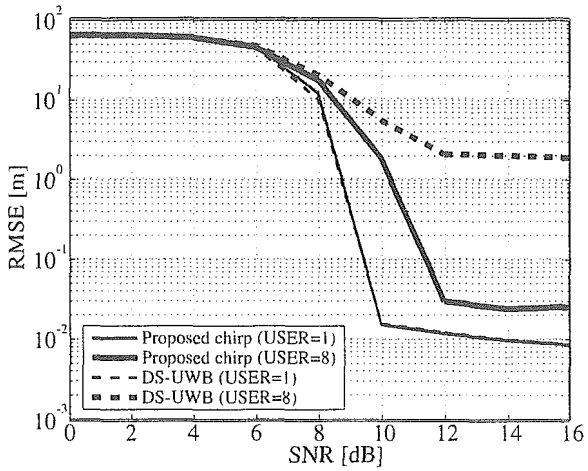

Figure 13: Performance of ranging to SNR.

Figure 13 shows RMSE characteristics to SNR in a single-user and a multi-user (8 users) environment. In a single-user environment, two systems have same performance. It is because they have same width of correlator output pulse, since they use same frequency bandwidth. Additionally, It is shown that the proposed system can perform ranging with fewer errors in multi-user environment.

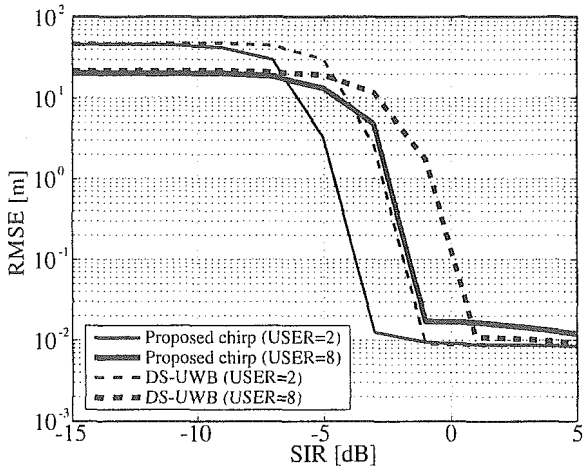

Figure 14: Performance of ranging to SIR.

By reason of assessing multiple access interference, RMSE characteristics to SIR is shown in Figure 14. It is assumed that there is no noise source. Because of low cross-correlation coefficients, as above-mentioned, it is shown that the proposed system achieves better ranging performance in multi-user environment.

5. Conclusions

We have proposed a novel multiple access technique utilizing non-linear swept chirp waveforms. By assigning a distinct non-linear frequency sweep functions to users, it can enable multiple access. Furthermore, since the frequency used by each user hardly collides by using non-linear sweep functions, good correlation characteristics is achieved - low sidelobe of the auto-correlation and low cross-correlation coefficients. Therefore, the proposed system is robust in multi-user environment. Simulation results show that the proposed system can achieve better performance of communication and ranging in multi-user environment as compared with DS-UWB system.

In future, we intend to take into consideration the implementability and the realistic channel models.

References

[1] A. Springer, M. Huemer, L. Reindl, C. C. W. Ruppel, A. Pohl, F. Seifert, W. Gugler, and R. Weigel, "A robust ultra-broad-band wireless communication system using SAW chirped delay lines," *IEEE Transactions on Microwave Theory and Techniques*, vol. 46, pp. 2213–2218, December 1998.

[2] C. E. Cook, "Linear FM signal formats for beacon and communication systems," *IEEE Transactions on Aerospace and Electronic Systems*, vol. 10, pp. 471–478, July 1974.

[3] S.E.El-Khamy, "Efficient multiple-access communications using multi-user chirp modulation signals," in *IEEE 4th International Symposium on Spread Spectrum Techniques and Applications*, vol. 3, September 1996, pp. 1209–1213.

[4] E. Cano and D. S. McGrath, "TH-UWB and DS-UWB in lognormal fading channel and 802.11a interference," in *IEEE Personal, Indoor and Mobile Radio Communications*, vol. 4, September 2004, pp. 2978–2982.

[5] M. Welborn, T. Miller, J. lynch, and J. McCorkle, "Multi-user perspectives in UWB communications networks," in *IEEE Conference on Ultra Wideband Systems and Technologies*, 2002, pp. 271–275.

[6] S. Ida, K. Doi, and R. Kohno, "A study on non-linear swept chirp waveform for uwb multiple access communications," *IEICE Technical report*, vol. WBS2003-225, pp. 197–202, 2004.

[7] T. Collins and P. Atkins, "Nonlinear frequency modulation chirps for active sonar," *IEE Proceedings - Radar, Sonar and Navigation*, vol. 146, no. 6, pp. 312–316, December 1999.

TRANSMISSION POWER CONTROL OF UWB-PAN TO AVOID INTERFERENCE IN THE PRESENCE OF BOTH WIRELESS LAN AND PAN

Marie ENDO and Ryuji KOHNO
(Graduate School of Engineering, Division of Physics, Electrical and Computer Engineering,
Yokohama National University, Yokohama, Kanagawa, JAPAN,
{marie, kohno}@kohnolab.dnj.ynu.ac.jp)

ABSTRACT

This paper assumes an environment where IEEE802.11a and UWB wireless communication systems coexist, and proposes a method to avoid interference from UWB systems to IEEE802.11a. Since both UWB systems and IEEE802.11a utilize a common frequency spectrum, the UWB signal power affects the carrier-sensing of IEEE802.11a. As a result, the throughput of the latter degrades. In this paper, the transmission power of UWB is controlled to avoid interference to IEEE802.11a. By using cognitive radio technique implemented at the base station of IEEE802.11a and monitoring throughput of IEEE802.11a, the transmission power is controlled accordingly. Additionally, the value of each transmission power is optimized in order to maximize total throughput of both IEEE802.11a and UWB, and each throughput and carrier-sense error rate are calculated and compared.

1. INTRODUCTION

Ultra Wideband (UWB) wireless communication systems have attracted attention as a new system which enables low power consumption and high-speed communications, and whose adoption into international standardization of Wireless PAN (Personal Area Network), IEEE802.15.3a, has been discussed [1]. Since UWB uses ultra wideband, 3.1 ~ 10.6GHz frequency band, it influences communications of existing systems such as IEEE802.11a, one of the Wireless LAN (Local Area Network) systems, utilizing 5GHz band. In this paper, an IEEE802.11a network and UWB coexistence is assumed. UWB is prescribed a spectrum mask to limit transmission power by FCC (Federal Communications Commission). However, even if the UWB transmission power is restricted so as to satisfy the limit, it will potentially lead to interference.

Generally, IEEE802.11a uses carrier-sense as medium access control method [2], [3]. In the carrier-sense, a terminal decides whether or not it sends data frames after sensing usage of the channel to avoid collision of frames with other terminals. When the power sensed by terminal is over carrier-sense level, the channel is assumed to be busy and thus the frames are postponed temporally (The algorithm of carrier-sense is briefly shown in Fig. 1). Therefore, when the power of UWB is sensed instead of IEEE802.11a, the carrier-sense error rate increases and thus the opportunity of sending data from IEEE802.11a decreases. As a result, the throughput of IEEE802.11a degrades.

In this paper, monitoring the network on the basis of the cognitive radio concept enables interference avoidance to IEEE802.11a accordingly. Cognitive radio gives the best performance to users flexibly by learning the environment changes [4], [5]. In order to maintain the performance of IEEE802.11a, we control with a cognitive radio technique, the transmission power of UWB terminals if the actual throughput is below the desired level, a new algorithm that maximizes the total throughput of both IEEE802.11a and UWB is introduced in this paper. In more detail, the base station of IEEE802.11a having the capability of cognitive radio controls the transmission power of each UWB terminal when the degradation of throughput of IEEE802.11a is observed. Our proposal is applicable to commercialization since the influence to IEEE802.11a is minimized and spectrum efficiency of IEEE802.11a and UWB is improved only by implementing cognitive radio technique at base station of IEEE802.11a.

In the performance evaluation, we calculate the throughputs of both IEEE802.11a and UWB, as well as the carrier-sense error rates, through computer simulations, showing the effectiveness of the proposed methods. In this paper, throughput is defined as the time spent to send the whole amount of data.

This paper is organized as follows: Section 2 describes the network model assumed in this paper. Section 3 shows an algorithm for avoiding interference to IEEE802.11a with UWB transmission power control. Section 4 presents an optimization method of UWB transmission power. Section 5 evaluates the effectiveness of proposal method. Finally, in Section 6 we draw some conclusions.

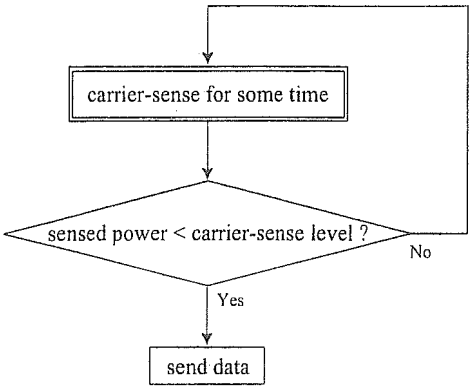

Fig. 1. Algorithm of carrier-sense.

2. NETWORK MODEL

Fig. 2 shows the network model assumed in this paper. In this model, IEEE802.11a and UWB coexist. The network includes a base station of IEEE802.11a (l_0), IEEE802.11a terminals (l_1, l_2, ⋯, l_m, ⋯, l_M) and UWB terminals (p_1, p_2, ⋯, p_n, ⋯, p_N).

In this paper, base station of IEEE802.11a possesses cognitive radio technique and can monitor the throughput of its network. Moreover, it also has a UWB hardware implemented and can control transmission power of UWB terminals. In addition, this base station is able to estimate the distance between each terminal.

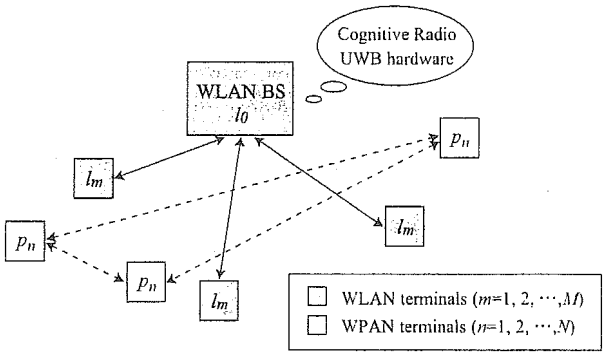

Fig. 2. Network Model.

3. ALGORITHM AVOIDING INTERFERENCE

An algorithm avoiding interference at the base station is shown in the following and Fig. 3.

1. Cognitive radio senses the throughput and the traffic volume of IEEE802.11a network. If the throughput does not satisfy the expected throughput, the base station performs as it follows.
2. The ranging function of UWB equipped at the base station estimates the distance between each terminal.
3. The base station calculates the optimal transmission power values for each UWB terminal as a function of the distance.
4. Finally, after changing each UWB transmission power to the respective optimal values, the communication is restarted.

The method to calculate each optimal value is explained Section 4.

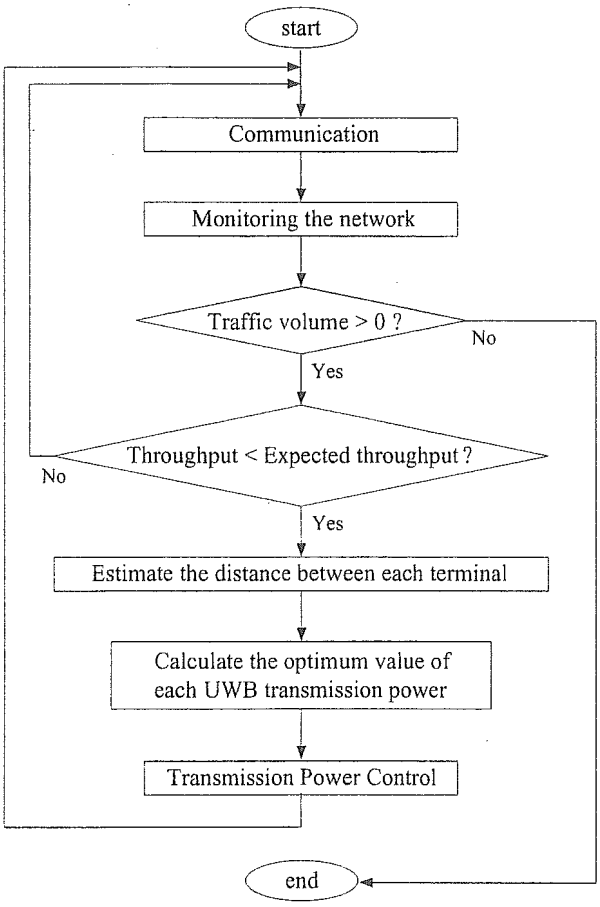

Fig. 3. Algorithm Avoiding Interference.

4. OPTIMIZATION

For throughput optimization of both IEEE802.11a and UWB, the throughput of each system is analyzed theoretically. Moreover, the parameters for optimization are indicated in Table 1.

Table 1. Parameters for Optimization

$d_{m,n}$	Distance between l_m and p_n [m]
$r_{n,n}$	Distance between p_n and p_n [m]
P_{s_n}	Transmission power of p_n [dBm]
λ	Wavelength in 5GHz band [m]
CL_l	Carrier-sense level of IEEE802.11a [dBm]
CL_p	Carrier-sense level of UWB [dBm]
P_{noise_l}	Noise power of IEEE802.11a [dBm]
P_{noise_p}	Noise power of UWB [dBm]
Th_l	Total throughput of IEEE802.11a [Mbps]
Th_p	Total throughput of UWB [Mbps]
$Th_{max\_l_m}$	Maximum total throughput of IEEE802.11a [Mbps]
$Th_{max\_p_n}$	Maximum total throughput of UWB [Mbps]
E_{l_m}	Carrier-sense error rate of l_m
E_{p_n}	Carrier-sense error rate of p_n

4.1. Throughput of IEEE802.11a

When an IEEE802.11a terminal catches the power of UWB terminal and assumes this power to be from its own system's terminal, the carrier-sense error occurs.

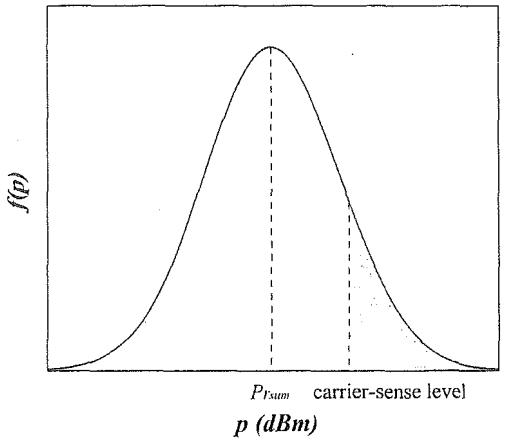

Fig. 4. Probability distribution of noise power.

The probability distribution of UWB power at the base station assumes normal distribution as Fig. 4 shows. The average is the sum of the received power of IEEE802.11a ($P_{r_{sum}}$) and the variance is the squared noise power ($P_{noise\_l}^2$). Since the shadowed area in Fig. 4 is probability that noise power is over the carrier-sense level, the dimension of this area corresponds to the error probability of carrier-sense. Probability density function $f(p)$ of the power p is shown as follows,

$$f(p) = \frac{1}{\sqrt{2\pi}P_{noise\_l}} e^{\frac{(p-P_{r_{sum}})^2}{2P_{noise\_l}^2}} \quad (-\infty < p < \infty). \quad (1)$$

Probability distribution function $F(p)$ of noise power over the normal distribution is

$$F(p) = \int_p^{\infty} f(p)dp = \frac{1}{2} erfc\left(\frac{p - P_{r_{sum}}}{\sqrt{2}P_{noise\_l}}\right). \quad (2)$$

Therefore, carrier-sense error rate E_{l_m} of terminal l_m is given by,

$$E_{l_m} = F(CL_l) = \frac{1}{2} erfc\left(\frac{CL_l - \sum_{n=1}^{N}\left(\frac{\lambda}{4\pi d_{m,n}}\right)^2 P_{s_n}}{\sqrt{2}P_{noise\_l}}\right), \quad (3)$$

where complementary error function $erfc(x)$ is approximated as follows [6]:

$$erfc(x) \cong 1 - \sqrt{1 - \exp\left(-\frac{4x^2}{\pi}\right)}. \quad (4)$$

Applying (4), (3) can be rewritten as:

$$E_{l_m} \cong \frac{1}{2}\left\{1 - \sqrt{1 - \exp\left[-\frac{4}{\pi}\left(\frac{CL_l - \sum_{n=1}^{N}\left(\frac{\lambda}{4\pi d_{m,n}}\right)^2 P_{s_n}}{\sqrt{2}P_{noise\_l}}\right)^2\right]}\right\}. \quad (5)$$

Finally, throughput of IEEE802.11a Th_l is obtained by,

$$Th_{lan} = \sum_{m=0}^{M} Th_{\max\_l_m}(1 - E_{l_m}). \quad (6)$$

4.2. Throughput of UWB

In this paper, the medium access method of UWB is compliant with IEEE802.11a. In contrast to the case of IEEE802.11a, UWB carrier-sense error occurs when UWB terminal cannot catch the power transmitted from other UWB terminals since the power is lower than the carrier-sense level. The carrier-sense error rate E_{p_n} of terminal p_n can be described as:

$$E_{p_n} = 1 - \frac{1}{2} erfc\left(\frac{CL_p - \left(\frac{\lambda}{4\pi r_{n,n}} \right)^2 P_{s_n}}{\sqrt{2} P_{noise\_p}} \right)$$

$$\cong 1 - \frac{1}{2}\left\{ 1 - \sqrt{1 - \exp\left[-\frac{4}{\pi} \left(\frac{CL_p - \left(\frac{\lambda}{4\pi r_{n,n}} \right)^2 P_{s_n}}{\sqrt{2} P_{noise\_p}} \right)^2 \right]} \right\}. \quad (7)$$

According to (7), the throughput of UWB Th_p is obtained by,

$$Th_p = \sum_{n=0}^{N} Th_{\max\_p_n} (1 - E_{p_n}). \quad (8)$$

4.3. Maximization of Total Throughput of Both IEEE802.11a and UWB

For the optimization of UWB transmission power, total throughput of both IEEE802.11a and UWB is maximized with the following objective function:

$$Th_l + Th_p \quad (9)$$

Each optimal value of UWB transmission power is decided in order to maximize (9) using nonlinear programming.

5. NUMERICAL RESULTS

The proposed algorithm is evaluated by computer simulation. In this paper, cognitive error by the cognitive radio and ranging error by UWB systems are not considered.

5.1. Simulation Parameters

The simulation parameters are shown in Table 2 ~ 4. Terminals are allocated on x-y coordinate at l_0=(0,0), l_1=(5,5), p_1=(0,5), p_2=(5,0) ([m]). The amount of traffic in downlink is equal to the total amount of traffic in uplink. Data size is 1500 octet and other parameters are compliant with IEEE802.11a. The MAC parameters of UWB in this paper are those of IEEE802.11a.

Table 2. System Parameters

M	Number of IEEE802.11a terminals	1
N	Number of UWB terminals	2
P_{noise_l}	Noise power of IEEE802.11a	-63 dBm
P_{noise_p}	Noise power of UWB	-17 dBm
P_{s1}	Initial value of transmission power	-5 dBm
P_{s2}	Initial value of transmission power	-5 dBm

Table 3. Parameters for IEEE802.11a

Bit Rate	24 Mbps	MAC header	24 octet
Preamble	16 μs	FCS	4 octet
PLCP header	4 μs	Data size	1500 octet
Slot time	9 μs	ACK size	14 octet
SIFS time	16 μs	CWmin	15
DIFS time	34 μs	CWmax	1023
Medium access method		DCF	
Carrier-sense level		-62dBm	

Table 4. Parameters for UWB

Bit Rate	480 Mbps	MAC header	24octet
Preamble	0.8 μs	FCS	4 octet
PLCP header	0.2 μs	Data size	1500 octet
Slot time	0.45 μs	ACK size	14 octet
SIFS time	0.8 μs	CWmin	15
DIFS time	1.7 μs	Cwmax	1023
Medium access method		DCF	
Carrier-sense level		-15dBm	

5.2. Simulation Results

Throughput characteristics of IEEE802.11a and UWB are shown in Fig. 5 and 6. The following cases are evaluated in these figures:

- without interference (only in Fig. 5)
- with interference from UWB, without power control
- with interference from UWB, with power control

It is noticeable that, due to the maximization of total throughput of IEEE802.11a and UWB, the throughput of UWB slightly degrades, whereas that of IEEE802.11a is improved about 2Mbps.

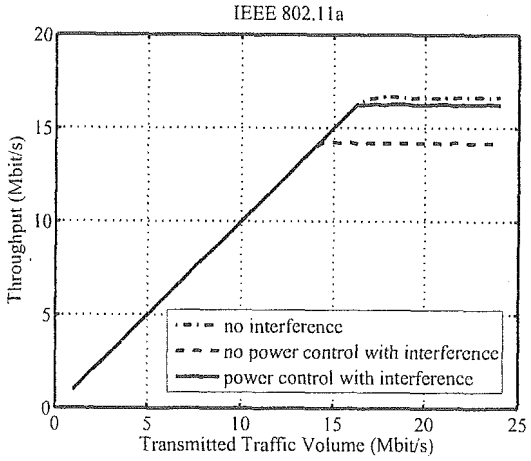

Fig. 5. Throughput of IEEE802.11a.

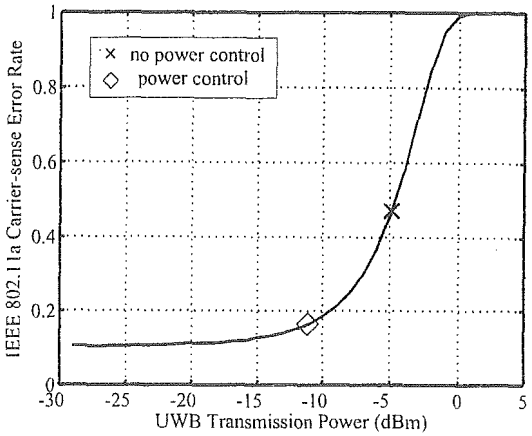

Fig. 7. Carrier-sense error rate of IEEE802.11a.

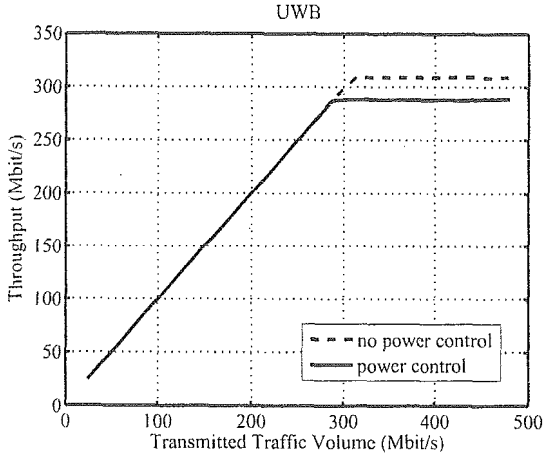

Fig. 6. Throughput of UWB.

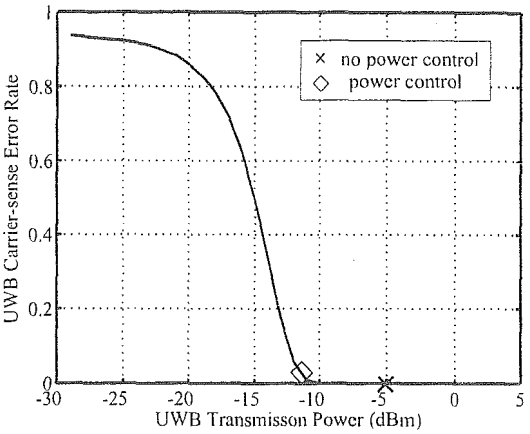

Fig. 8. Carrier-sense error rate of UWB.

The carrier-sense error rates of both systems against the average UWB transmission power are shown in Fig. 7 and 8. Although the UWB carrier-sense error rate slightly increases, the controlled UWB transmission power minimizes the total carrier-sense error rate for both systems, thus the total throughput is maximizes. Consequently, the controlled UWB transmission power can be considered to be an optimal solution.

6. CONCLUSIONS

In this paper, an algorithm avoiding interference from IEEE802.11a to UWB with cognitive radio in an environment where the two systems coexist is proposed. Improvement on the throughputs of both IEEE802.11a and UWB by calculating and controlling optimal value of each UWB terminal's transmission power is shown.

In our future studies, addition of other systems to the proposed network and reduction of the calculation complexity shall be considered. Moreover, cognition error of cognitive radio will also be considered.

7. REFERENCES

[1] Ryuji Kohno, "Principle and Emotion of Ultra Wideband (UWB) Wireless Communications Based on Impulse Radio," Technical Report of IEICE, DSP2001-80, July 2001.

[2] ANSI/IEEE Std 802.11, "Information technology-Telecommunications and information exchange between systems- Local and metropolitan area networks- Specific requirements- Part 11: Wireless LAN Medium Access Control (MAC) and Physical Layer (PHY) Specifications," 1999.

[3] Hideaki Matsue, Masahiro Morikura, "802.11 High-speed Wireless LAN Textbook," IDG JAPAN.

[4] John Polson, "Cognitive Radio Applications in Software Defined Radio," in Proceedings of Software Defined Radio Technical Conference, Phoenix, Arizona, November 2004.

[5] Joseph Mitola III and Gerald Q. Maguire, Jr. "Cognitive Radio: Making Software Radios More Personal," IEEE Personal Communications, August 1999.

[6] Marie Endo, Kyoichi Obana, Motoko Taniguchi, Kentaro Ikemoto, Ryuji Kohno, "A Study on Transmission Power Control of UWB Terminals to Avoid Interference to Wireless LAN Based on Cognitive Radio Concept," Technical Report of IEICE, SR04-28, pp.51-56, March 2005.

Interference Reduction Using Novel Pulse Set Based on Hermite Polynomials for UWB-WPAN Systems

Hiroki Harada and Ryuji Kohno
Division of Physics, Electrical and Computer Engineering, Yokohama National University
79–5 Tokiwadai, Hodogaya, Yokohama, 240–8501, Japan.
Tel.: +81-45-339-4116 Fax: +81-45-338-1176
E–mail: hhiroki@ieee.org, kohno@ynu.ac.jp

Abstract— **In this paper, a combination of a pulse shape hopping (PSH) and a time hopping (TH) for ultra wideband (UWB) systems is proposed as an effective method for reducing both a multi-user interference (MUI) and an inter-symbol interference (ISI). Furthermore, we consider applying *modulated and modified Hermite pulses* (MMHP). MMHP is extended to a novel pulse set referred to as *limited bandwidth MMHP set* in order to reduce various interferences, which is composed of pseudo-orthogonal pulses that have both good auto-correlation characteristics in all orders and low cross-correlation characteristics between different orders. Proposed pulse set also have some specific notches, which can be used to reduce a narrow-band interference (NBI). Simulation results show significant improvements by using proposed methods.**

Index Terms— **UWB-WPAN, limited bandwidth MMHP, pulse shape hopping, interference reduction**

I. Introduction

Ultra wideband (UWB) communication has been studied actively since the Federal Communications Commission (FCC) authorized civilian use of UWB on February 2002 [1]. UWB communication systems will be severely limited to a maximum transmission power for co-existing narrowband and wideband wireless communication systems already operating in dedicated frequency bands. Thus the FCC provides a spectral mask that regulates the used frequency from 3.1GHz to 10.6 GHz for wireless personal area network (WPAN).

The performance degradation in terms of bit error probability is mainly caused by three factors in UWB-WPAN [2]. The first is a multi-user interference (MUI) from other users of UWB system, in other words, it is an interference from asynchronous piconets. The second is an inter-symbol interference (ISI), which is caused by delay spreading. The third is a narrow-band interference (NBI), which is interference from co-existing narrowband and wideband communication systems, for instance, 5GHz-band WLAN system. In UWB-WPAN system, it is required that UWB system reduces these interferences effectively.

We propose a pulse shape hopping (PSH) which is a method of hopping waveforms to each transmitting times for reducing the effect of ISI in the case of a high speed communication [3]. Since each users have different hopping codes, MUI can be reduced by using a combination of PSH and time hopping (TH).

In addition, we design a novel pulse set which occupy the same bandwidth in all orders in order to satisfy the spectral mask effectively. Our proposed modulated and modified Hermite pulses (MMHP) pulse set called "limited bandwidth MMHP set" is composed of pseudo-orthogonal pulses to each different order, and auto-correlation characteristics of the proposed MMHP are good. Furthermore, the cross correlation value of the proposed MMHP several orders apart are always low, and the spectrum of the MMHP has notches whose number is the same as the order. Interferences by delayed signal or other user's signal can be reduced by using these correlation characteristics of the proposed MMHP.

Furthermore, our proposed system can resolve the problem of co-existence between UWB system and other systems, for instance, WLAN system called "IEEE802.11a" which occupies 5GHz band [4, 5]. We use notches of the proposed MMHP to reduce an overlap between the spectrum of the UWB and the spectrum of the WLAN so that NBI are reduced effectively.

This paper is organized as follows. In Section II, we outline our proposed UWB system using the limited bandwidth MMHP set. In section III, numerical comparison between the proposed system and the conventional UWB system is presented specifically. Finally, conclusions and future works are remarked in Section IV.

II. Proposed TH-UWB System Using Novel Pulse Set

In this section we explain our proposed UWB system using a novel pulse set based on MMHP.

A. Proposed Pulse Set Design(Limited Bandwidth)

In TH-UWB system, an user sends pulses in a certain timing with an unique TH sequence. In our proposed system, users utilize improved MMHP of various orders in contrast to the case of conventional TH-UWB systems. The MMHP and their characteristics are described below.

The *Hermite polynomials* that were known in the past are given by

$$\begin{aligned} h_{e_0}(t) &= 1 \\ h_{e_n}(t) &= (-1)^n e^{\frac{t^2}{2}} \frac{d^n}{dt^n}(e^{-\frac{t^2}{2}}), \end{aligned} \tag{1}$$

where n is the order of the Hermite polynomials. Different orders of these Hermite functions are not orthogonal to each other. Consequently, these functions are modified to become

orthogonal and are represented as follows [6–8].

$$h_n(t) = e^{-\frac{t^2}{4}} h_{e_n}(t) = (-1)^n e^{\frac{t^2}{4}} \frac{d^n}{dt^n}(e^{-\frac{t^2}{2}}). \quad (2)$$

The MHP whose orders are different are orthogonal to each other when they are synchronized exactly.

However, FCC spectral mask regulates the used frequency from 3.1GHz to 10.6 GHz for UWB-WPAN. Hence, the MHP which have low frequency component is inapplicable pulses for UWB-WPAN [3].

The MHP which are multiplied by a sine wave of frequency equal to f_c are represented as follows.

$$h_{m_n}(t) = h_n(t)\sin(2\pi f_c t) = (-1)^n e^{\frac{t^2}{4}} \frac{d^n}{dt^n}(e^{-\frac{t^2}{2}})\sin(2\pi f_c t). \quad (3)$$

We use this formula to produce the MMHP.

The MMHP occupies the specified band for UWB-WPAN. Additionally, the MMHP is efficient waveform as a transmitted pulse for TH-UWB since the MMHP of various orders can be generated by an oscillator and the simple MHP generater [9].

However, there are some problems. The bandwidth of the MMHP extends as the number of order increases. Therefore, the MMHP of higher order cannot be used in the case of considering the spectral mask [3]. Moreover, different orders of the MMHP have different bandwidth respectively. Since, robustness against multipath fading varies with the order of the transmitted MMHP.

So, we improve the waveform to resolve these problems. (3) can be transformed as follows.

$$h_{l_n}(t) = N_n(-1)^n e^{\frac{(\frac{t}{t_p})^2}{4}} \frac{d^n}{dt^n}(e^{-\frac{(\frac{t}{t_p})^2}{2}})\sin(2\pi f_c t). \quad (4)$$

N_n is a normalizing parameter and t_p is a parameter which controls the pulse width. If the t_p increases, the bandwidth of the pulse becomes narrower. Consequently, the bandwidth can be fit into the bounds of the spectral mask if the MMHP of higher order are used (see Fig. 1). The value of t_p is fixed up suitably to each orders so that the MMHP of different orders have the same bandwidth. We call the proposed pulse set "*limited bandwidth MMHP* (LB-MMHP) set".

The novel set of LB-MMHP that is generated in this way has the following characteristics.

- The LB-MMHP whose orders are different are pseudo-orthogonal to each other when they are synchronized exactly.
- The LB-MMHP has sharp auto-correlation characteristics in all orders as contrasted with the conventional set of the MMHP.
- The cross-correlation between different orders is low and independent of delay time.
- Variance values of cross-correlation functions are always lower than variance values of auto-correlation functions.
- The spectrum of the LB-MMHP has notches whose number is the same as the order.

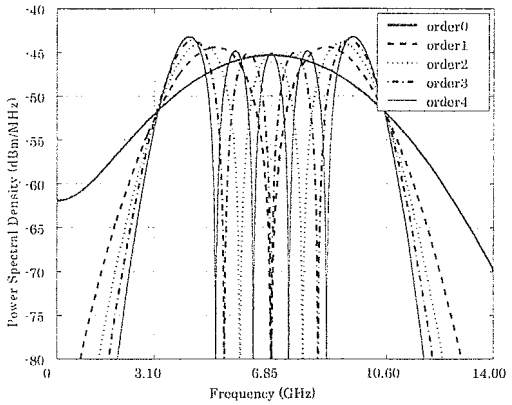

Fig. 1. The frequency domain representation of the limited bandwidth MMHP set: order 0,1,2,3,4.

B. Correlation Characteristics Analysis

As follows, we confirm correlation characteristics of the LB-MMHP set.

The correlation value of the proposed LB-MMHP $C_{m,n}(\tau)$ is given by

$$C_{m,n}(\tau) = \int_{-\infty}^{\infty} h_{l_m}(t) \cdot h_{l_n}(t-\tau)dt. \quad (5)$$

Figure 2 shows the auto-correlation characteristic of the LB-MMHP based on (5). Auto-correlations of all orders have the same peaks and low auto-correlation values around delay time 0.

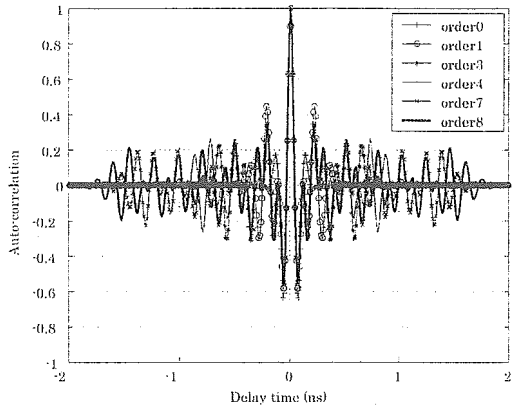

Fig. 2. An auto-correlation characteristic of the MMHP of order ranging from 0 to 8.

On the other hand, Fig. 3 shows the cross-correlation characteristic of the LB-MMHP based on (5). We can see that the cross-correlation between different orders is lower than the auto-correlation and independent of delay time.

Additionally, Table 1 shows variance values of correlation